Macromolecular Research, Vol. 24, No. 10, pp 900-908 (2016)
DOI 10.1007/s13233-016-4131-4

www.springer.com/13233
pISSN 1598-5032 eISSN 2092-7673

In Situ Polymerized Poly(butylene succinate-*co*-ethylene terephthalate)/Hydroxyapatite Nanocomposite with Adjusted Thermal, Mechanical and Hydrolytic Degradation Properties

Hadi Shirali[1], Mehdi Rafizadeh*[,2], and Faramarz Afshar Taromi[3]

[1]*Department of Polymer Engineering and Color Technology, Amirkabir University of Technology, Iran*
[2]*Corresponding author, Department of Polymer Engineering and Color Technology, Amirkabir University of Technology, PO Box 15875-441, Tehran, Iran*
[3]*Department of Polymer Engineering and Color Technology, Amirkabir University of Technology, Iran*

Received April 25, 2016; Revised July 5, 2016; Accepted July 30, 2016

Abstract: New nanocomposites of poly(butylene succinate-*co*-ethylene terephthalate)/nano hydroxyapatite were synthesized using two-step *in situ* polycondensation. The composition, microstructure, morphology and dispersion of nanoparticles in the nanocomposites were studied using proton nuclear magnetic resonance (^{1}H NMR), Fourier transform infrared spectroscopy (FTIR), scanning electron microscopy (SEM) and transmission electron microscopy (TEM). It was found that presence of nano hydroxyapatite catalyzes the reaction and there is a chemical bond between nanoparticles and polymer which leads to a good particle dispersion but it doesn't affect molecular sequence length. Nanocomposites' thermal properties evaluated by differential scanning calorimetry (DSC) and X-ray diffraction (XRD), showed that crystallinity and crystallite size slightly decrease with the nanoparticles weight fraction. Moreover, the elastic modulus slightly increases and tensile strength and elongation at break decrease with the nanoparticles weight fraction according to dynamic mechanical thermal analysis (DMTA) and tensile analysis. Introducing nano hydroxyapatite increases the hydrolytic degradability dramatically because of the presence of hydrophilic nanoparticle and lower crystallite size.

Keywords: copolyester, nanocomposite, poly(butylene succinate-*co*-ethylene terephthalate), nano hydroxyapatite, degradability.

Introduction

Nowadays, using biodegradable polymeric materials as therapeutic devices including artificial prosthesis, controlled drug release devices and 3D scaffolds for tissue engineering has been progressively increased.[1] Hence, researchers have focused on improving thermomechanical and biocompatibility properties of new biodegradable materials, using various methods such as copolymerization, mixing, adding inorganic nano-material to polymeric matrix and biomimetic.[2,3] Designing nanocomposite based on bone structure, as a good example of nanocomposites, is perceived to be beneficial bone. It is composed of two major phases at the nanoscale level namely, protein and inorganic mineral. The protein provides tensile strength and flexibility, whereas the minerals provide toughness and rigidity to the bone.[4] Aliphatic polyesters which are biodegradable materials, is known as one of the most promising because of their biodegradability which decompose to non-toxic and water-soluble oligomers.[5-8] Among them, good thermomechanical properties such as crystallinity, high melting point and good processability of poly(butylene succinate) (PBS), make it a suitable candidate to be used in many fields.[9] Due to low cost and high physical properties of aromatic polyesters such as poly(ethylene terephthalate) (PET), preparation of aliphatic-aromatic copolyesters is an approach to reach improved properties.[10] Several aliphatic-aromatic copolyesters have been synthesized so far. Wang *et al.*[11] prepared poly(butylene succinate-b-diethylene glycol succinate) copolyester using reactive blending. The glass transition temperature and cold crystallization temperature increased, while melting temperature and the crystallinity decreased with the increase in comonomer content. Recently, we synthesized poly(butylene succinate-*co*-ethylene terephthalate) random copolyester *via* direct polycondensation of bis(2-hydroxy ethyl terephthalate) (BHET) and bis(4-hydroxy butyl succinate) (BHBS).[12] The incorporating BHET into main chain leads to a decrease in the crystallinity, melting point, elastic modulus and hydrolytic degradation rate but dramatically increases the elongation at break up to

*Corresponding Author. E-mail: mehdi@aut.ac.ir

500%. Therefore, the resulted copolyester could be used to mimic the bone structure.

Beside copolymerization, making nanocomposites using calcium phosphates like hydroxyapatite (HA) and tricalcium phosphate (β-TCP) is highly attractive for many medical applications because of their excellent biocompatibility and osteoconductivity.[13,14] Among them, HA have excellent biocompatibility, osteoconductivity, osteoinductivity and low degradation rate, due to its natural bone like structure and chemical composition. However, brittleness and difficulty in shaping of HA limit its applications. Moreover, HA powders tend to agglomerate due to its high surface energy, and it is hard to make well dispersed nanocomposites.[15]

The aim of this study is to synthesize and characterize a novel nanocomposite of poly(butylene succinate-*co*-ethylene terephthalate)/nano hydroxyapatite (PBSET-nHA). The molecular structure, nanoparticle dispersion, morphology and their effects on thermomechanical properties and biodegradability were investigated by various methods. To the best of our knowledge, thermal and mechanical properties of resulted nanocomposite should be higher than PBSET due to the introduction of nHA into the copolyesters.

Experimental

Materials. Ethylene glycol (EG) and terephthalic acid (TA) were supplied by Shahid Toundgoyan Petrochemical Complex, Mahshar, Iran. Succinic acid (SA), butylene glycol (BG), titanium butoxide (TBT), as polycondensation catalyst, and highly pure chloroform, as solvent for intrinsic viscosity measurement, were bought from Merck Co., Darmstadt, Germany. Nano hydroxyapatite (nHA) was purchased from DK-nano Co, China.

Synthesis of Nanocomposites. First, bis(4-hydroxybutyl) succinate (BHBS) and Bis(2-hydroxyethyl) terephthalate (BHET) were synthesized by esterification of SA, BG, ET and EG, using a custom-built laboratory-scale reactor as described elsewhere.[12] Then, BHBS, BHET, TBT, and PPA and nHA (if necessary) were mixed and *in situ* polycondensation step was performed. Mixture temperature was increased to 265 °C and 250 °C for neat polymer, and nanocomposites, respectively, and vacuum was and applied.[12] The end of this step was determined by measuring mixer torque. Scheme I shows the synthesis route of the nanocomposites.

Characterization. The intrinsic viscosity of nanocomposites was calculated using 0C type Ubbelohde and chloroform as solvent at 25±0.1 °C. Eq. (1) was used to approximate number average molecular weight (M_n):[9]

$$\overline{M}_n = 3.29 \times 10^4 \times [\eta]^{1.54} \quad (1)$$

^{1}H NMR spectra of nanocomposites were recorded by Brucker Avance (Switzerland) 400 at 400 MHz and 25 °C. Tetramethylsilane (TMS) and $CDCl_3$ were used as reference and solvent, respectively.

Infrared spectra were recorded on a Nexus 670 spectrophotometer from Nicolet Co. (Waltham, MA) at room temperature. The samples were prepared by mixing 1 mg of products with 100 mg of KBr.

Scanning electron microscope images (SEM) were recorded with a VEGA3 SBU variable pressure (Tescan, Kotoutovice, Czech Republic) at an accelerating voltage of 20 keV. Samples were coated with gold using a Denton Desk II sputter coater (Moorestown, NJ).

TEM image of nanocomposites were imaged using a Hitachi H8000 Scanning Transmission Electron Microscope with an acceleration voltage of 200 kV. Samples were microtomed to thin slices (< 200 nm) by a cryomicrotome with a glass knife (Leica UC7/FC7 cyro-ultramicrotome) in liquid nitrogen.

Thermal and Mechanical Properties. 4-10 mg of samples

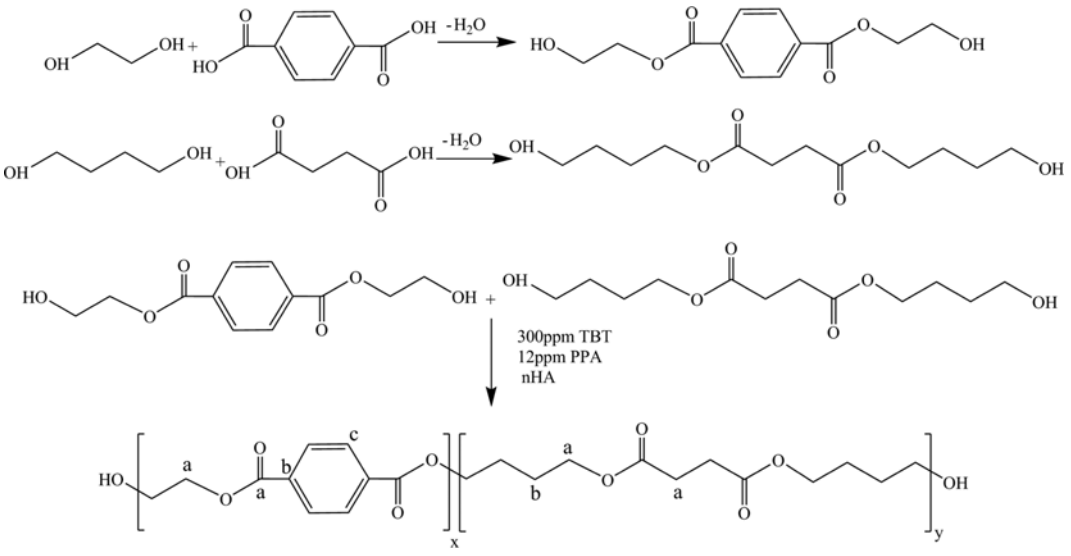

Scheme I. Schematic of the preparation of PBSET10-nHA nanocomposites.

was used to perform DSC analysis by Mettler-Toledo 822e instrument (Columbus, OH). Thermal history of samples was removed by melting them in 160 ºC for 2 min. Then, the samples were cooled to -50 ºC and then heated again to 160 ºC to obtain DSC thermograms. The cooling and heating rate were 10 ºC/min.

An EQuinox 3000 model was used to record XRD pattern with tube voltage, tube current and Cu$K\alpha$1 irradiation 40 kV, 30 mA and λ = 0.1541874 nm, respectively. The nanocomposites were hot-pressed to film at 120 ºC, cooled to room temperature with the rate of 10 ºC/min and scanned in the fixed-time mode for 2θ in the range 4º-120º and.

The samples were hot-pressed to make sheets (45×15×3 mm^3) and used to performed DMTA analysis by TA Instrument, model DMA983. Temperature sweep in tensile mode was carried out from -50 ºC to 150 ºC at 1 Hz with heating rate of 5 ºC/min.

Hot-pressed samples were used to measure tensile properties of the nanocomposites. The crosshead speed and temperature were 50 mm/min and 25 ºC, respectively.

Degradability. 1 M NaOH aqueous solution was used to measure hydrolytic degradation of samples. Hot-pressed film samples with dimension of 10×10×0.1 mm^3 were weighted (W_i) and soaked in the solution at 37 ºC. At each time point, samples were removed from solution, washed with deionized (DI) water three times, dried under vacuum at 40 ºC, and weight of the dried sample (W_t) was recorded. The percent weight loss was calculated using the following equation:

$$W_{loss} = \frac{W_i - W_t}{W_i} \times 100 \quad (2)$$

Results and Discussion

PBSET10 and PBSET10-nHA nanocomposites with different amount of nHA were produced according to the experimental part and summarized in Table I. The mole percentage of BHET and weight percentage of nHA were shown with the numbers next to the PBSET and nHA, respectively. 10 mole percent of BHET was selected based on the previous study due to having optimum crystallinity and hard segment which leads to highest tensile elongation, good degradability. Incorporation of nHA leads to decrease in polycondensation temperature up to 15 ºC because of the presence of Ca in nano hydroxyapatite structure which acts as catalyst.[16,17] Moreover, OH groups of nHA could react with monomers which lead to grafted copolymer, and crosslinking may happen if more than one OH groups of a nHA crystal react with chains.[18]

^{1}H NMR spectra of the nanocomposites are shown in Figure 1 and used to investigate their structure. The shifts were

Table I. Composition, Molecular Weight, and Carboxyl end Group of Synthesized Samples

Sample	BHET/BHBS/nHA	COOH (meq/kg)	[η] (dL/g)	M_n (g/mol)
PBSET10-nHA0	10:90:0	31	1.22	44,900
PBSET10-nHA1	10:90:1	23	1.25	46,500
PBSET10-nHA2.5	10:90:2.5	20	1.28	48,200
PBSET10-nHA5	10:90:5	21	1.29	48,900

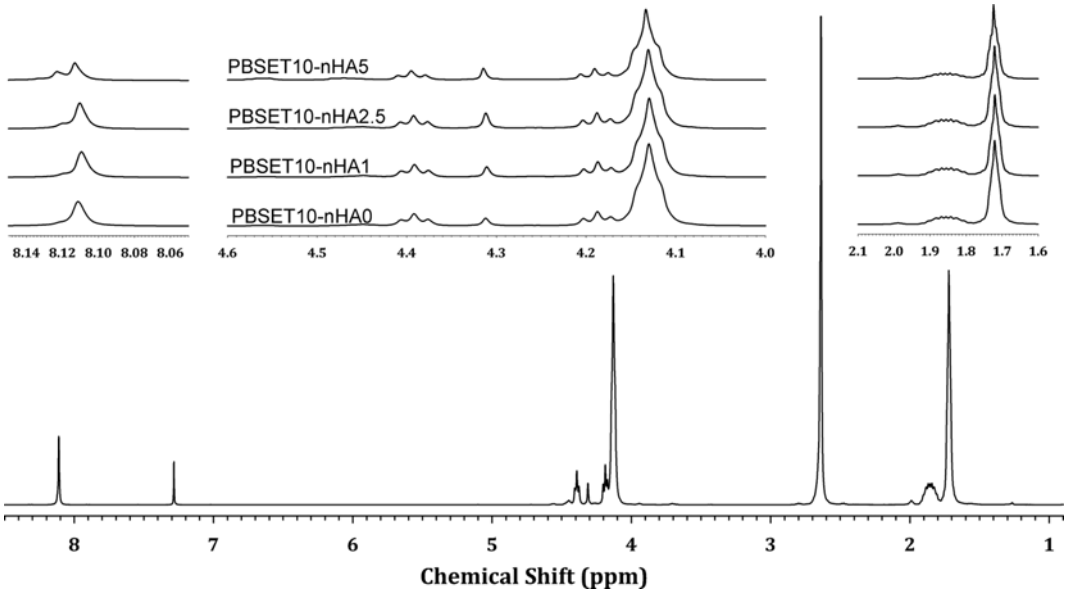

Figure 1. ^{1}H NMR spectra of nanocomposites.

assigned as: $^{B}H_b$ (1.77 ppm), $^{S}H_a$ (2.65 ppm), $^{B}H_a$ (4.13 ppm), $^{E}H_a$ (4.84 ppm), and $^{T}H_c$ (8.11 and 8.12 ppm),[19-22] which ^{S}H, ^{B}H, ^{T}H, and ^{E}H show hydrogen of SA, BG, TA, and EG, respectively and the subscripts are shown in the Scheme I. As it can be seen, a peak is appeared at 8.12 ppm which is related to $^{T}H_c$ and its intensity increases with the nanoparticles weight fraction. The reaction of OH group of nHA with oligomers leads to create a new bond which means grafting and crosslinking were happened in nanocomposite. Moreover, it will affect dispersion of nanoparticle in polymeric matrix which will be discussed in TEM test.

The degree of randomness, mean length of sequences, and dyad sequence distribution could also be estimated using the ^{1}H NMR spectra. There are eight signals that are related to methylene group of EG and BG groups, which is named "a" in Scheme I: Terephthalate ethylene terephthalate, TET, at 4.406 ppm, terephthalate ethylene succinate, TES, at 4.392 ppm, succinate ethylene terephthalate, SET, at 4.376 ppm, succinate ethylene succinate, SES, at 4.312 ppm, terephthalate butylene terephthalate, TBT, at 4.203 ppm, terephthalate butylene succinate, TBS, at 4.187 ppm, succinate butylene terephthalate, SBT, at 4.172 ppm, and succinate butylene succinate, SBS, at 4.130 ppm. The degree of randomness could be estimated using the areas under these eight peaks, defined as f_{TET}, f_{TES}, f_{SET}, f_{SES}, f_{TBT}, f_{TBS}, f_{SBT}, and f_{SBS}, respectively. First, the molar ratios of ethylene terephthalate groups, P_{ET}, butylene terephthalate groups, P_{BT}, ethylene succinate groups, P_{ES}, and butylene succinate groups, P_{BS}, are calculated *via* the following equations:

$$P_{ET} = (f_{TES}+f_{SET})/2+f_{TET} \quad (3)$$

$$P_{BT} = (f_{TBS}+f_{SBT})/2+f_{TBT} \quad (4)$$

$$P_{ES} = (f_{TES}+f_{SET})/2+f_{SES} \quad (5)$$

$$P_{BS} = (f_{TBS}+f_{SBT})/2+f_{SBS} \quad (6)$$

The number-average sequence length of ET, BT, ES, and BS units (L_{nET}, L_{nES}, L_{nBT}, and L_{nBS}, respectively) are obtained using the following equations:

$$L_{nET} = 2P_{ET}/(f_{TES}+f_{SET}) \quad (7)$$

$$L_{nES} = 2P_{ES}/(f_{TES}+f_{SET}) \quad (8)$$

$$L_{nBS} = 2P_{BS}/(f_{TBS}+f_{SBT}) \quad (9)$$

$$L_{nBT} = 2P_{BT}/(f_{TBS}+f_{SBT}) \quad (10)$$

Finally, the degree of randomness (R) is calculated from:

$$R = 1/L_{nAr}+1/L_{nAl} = 2/(L_{nBT}+L_{nET})+2/(L_{nBS}+L_{nES}) \quad (11)$$

If the value of R is close to 1.0, random copolyester is produced. The results are shown in Table II.

The results show that the molar ratio of TPA:SA in feed and nanocomposites are more or less equal. EG:BG molar ratio in nanocomposites is more than the feed, which is attributed to competition between BG and EG end groups and shows that EG has more reactivity than BG and remains in the reaction. Moreover, incorporation of nHA doesn't affect L_{nET}, L_{nBT}, L_{nBS}, and randomness but increases ethylene succinate length (L_{nES}).

To further investigate the grafting of polymer to nHA, all nanocomposites were dissolved in chloroform, centrifuged and washed with chloroform to separate nHA-grafted polymer. Un-grafted polymer remains in solution and nanoparticle precipitated. Then, FTIR test was performed on pure nHA and dried extracted nHA from nanocomposites and the results are shown in Figure 2. The pure nHA spectrum shows five peaks at 471, 563, 601, 1036, and 1096 cm^{-1} which are assigned to the PO_4^{3-} bending mode. The peaks at 963, 1417, and 3567 cm^{-1} are attributed to stretching PO_4^{3-}, CO_3^{-}, and structural OH, respectively. There are two peaks at 1632 and 3429 cm^{-1} which is due to the presence of adsorbed water.[23] All extracted nanoparticles show the characteristic peaks of polyesters. The sharp peak at 1732 cm^{-1} is corresponded to C=O carbonyl group in ester band. Two sharp peaks at 1161 and 1275 cm^{-1} are also related to the aromatic and aliphatic C-O bond in the ester group, respectively. Peaks at 2961 and 2858 cm^{-1} are attributed to the asymmetric and symmetric stretching vibrations of methylene groups. The out of plane C-H bending of aromatic ring could be found at 732 cm^{-1}.[24] These peaks demonstrate bonds among polymer and nHA. Existence of bonds among polymer and nHA is in agreement with ^{1}H NMR results. Moreover, the intensity of structural OH peak reduced which might be due to the reaction of this group with polymer.

The SEM and TEM images of the PBSET10-nHA5 nanocomposite are given in Figure 3. As shown, nHA particle size is around 88 nm and its dispersion is very good and there is no agglomeration. It can be concluded that the main reason of good dispersion is the presence of chemical bond between nHA and polymer which can overcome the interaction among particles.[25]

Table II. H NMR Results of All Samples

Sample	Feed Ratio of BHET:BHBS:nHA	TA:SA	EG:BG	L_{nET}	L_{nBT}	L_{nES}	L_{nBS}	R
PBSET10-nHA0	10:90:0	9.4:90.6	13.1:86.9	1.62	1.59	1.80	17.77	0.73
PBSET10-nHA1	10:90:1	8.6:91.4	13.8:86.2	1.58	1.67	1.92	16.46	0.72
PBSET10-nHA2.5	10:90:2.5	8.4:91.6	16.3:83.7	1.65	1.78	2.50	16.39	0.69
PBSET10-nHA5	10:90:5	9.5:90.5	13.6:86.4	1.58	1.78	2.52	19.70	0.69

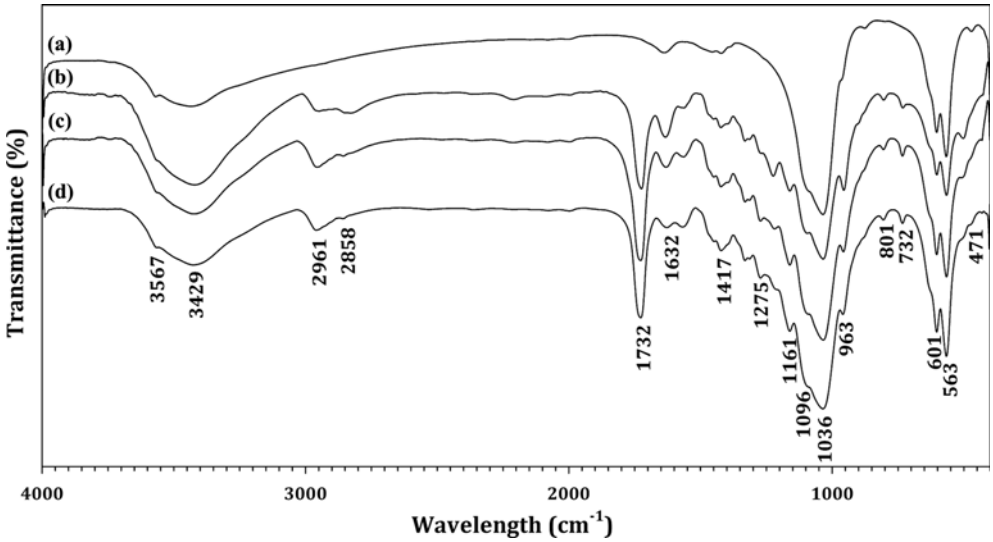

Figure 2. FTIR spectra of (a) pure nHA, (b), (c), and (d) extracted nHA from PBSET10-nHA1, PBSET10-nHA2.5, and PBSET10-nHA5, respectively.

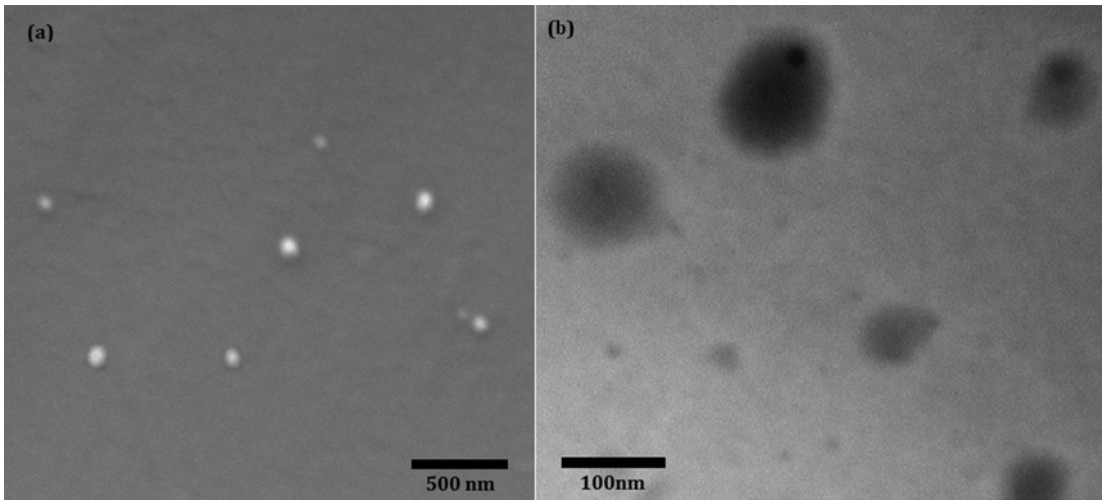

Figure 3. (a) SEM and (b) TEM image of PBSET10-nHA5 nanocomposite.

It is known that the nHA tends to aggregate in the solutions due to the inter-particle Van der Waals interaction as well as the hydrogen bonding[26] which lead nanoparticles to precipitate from colloid. Figure 4 shows time-dependent phase behavior of the PBSET10 nanocomposites dissolved in the chloroform after one week. It is interesting to note that the solutions show excellent phase stability due to the surface-grafted nHA to PBSET10, which is freely soluble in chloroform. These results can confirm the presence of chemical grafting between PBSET10 and nHA.

Heating DSC thermograms of nanocomposites and related results are shown in Figure 5 and Table III, respectively. The glass transition temperature (T_g) of nanocomposites is lower than neat PBSET10. Previous studies[27,28] have indicated that in the presence of fillers, fillers-matrix surface interactions affect the dynamics of polymers near fillers surfaces which

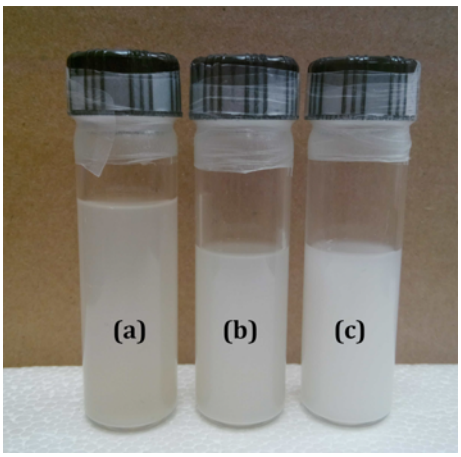

Figure 4. Phase behavior of (a) PBSET10-nHA1, (b) PBSET10-nHA2.5, and (c) PBSET10-nHA5 solutions after one week.

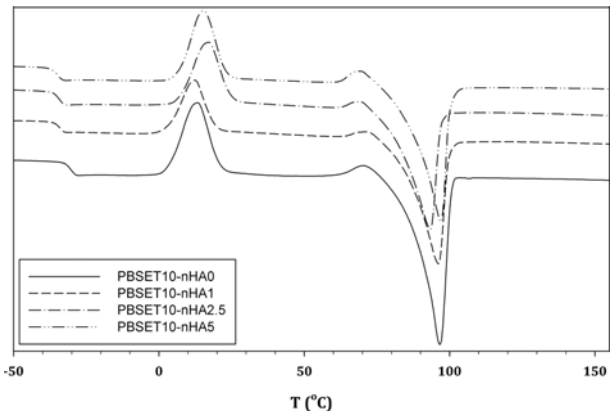

Figure 5. Heating DSC thermograms of all samples.

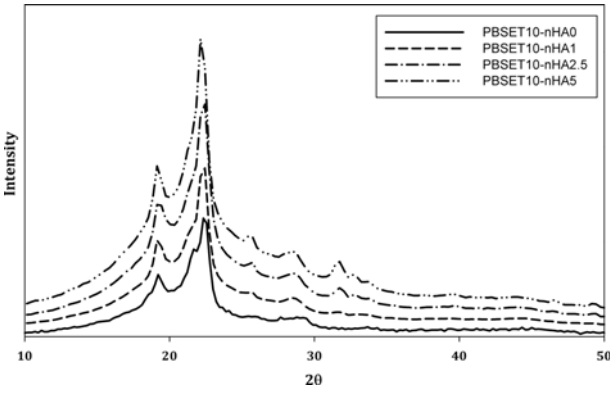

Figure 6. XRD curves of all nanocomposites.

leads to the increase or decrease in T_g. When the polymer-filler interactions are attractive, dynamics of polymer slow down (increased T_g) and if the interactions are repulsive, dynamics accelerate (decreased T_g). If the polymer wets the filler or not this result remains true. Thus, our results indicate that the interaction at the filler-polymer interface may be repulsive in nature. A sharp endothermal peak is observed in PBSET10 thermgram at 96.6 °C which is attributed to melting point. Introducing nanoparticles to the polymer leads to decrease and then increase in the melting temperature. Moreover, broadening of the melting peak shows that crystallization behavior change with incorporation of nHA. It is well-known that incorporating nHA in the polymer matrix will increase the melt viscosity of nanocomposites, which withstand the polymer chains motion to rearrange regularly to form crystals.[29] Moreover, Viscosity of nanocomposites increases with grafting chain to the nanoparticles. In spite of viscosity, nucleating sites increases with the nanoparticles weight fraction, and as a result, crystal number increases and crystallite size decreases. Therefore, competition between these two parameters by incorporating nHA leads to decrease in crystallinity and PBSET10-nHA5 shows the highest crystallinity in nanocomposites. Also, all theromgrams show a cold crystallization peak (T_{cc}) at about 10-20 °C which is because of very quick cooling rate. A crystalline polymer cannot be fully crystallized if it cools down quickly from the molten state. So, if it heated again above its T_g, crystallization occurs, which is called cold crystallization.

Figure 6 shows XRD patterns of PBSET10 and its nanocomposites. The nanocomposite crystallite is monoclinic in α form,[19,30] which show four diffraction peaks from the (002), (012), (110), and (111) planes at $2\theta \approx 19.6$, 21.8, 22.6, and 29.1°, respectively. There are three new peaks at $2\theta \approx 25.8$, 31.7, and 32.7° which are attributed to (002), (211) and (300) planes of nHA crystal, respectively.[31] The diffraction peaks of nanocomposites are the same, which shows they have one crystalline form. Diffraction peaks were deconvoluted using Pearsn VII equation which shows that full width at half maximum of peaks (B) increase with nHA content. The mean crystal sizes of (hkl) plane (L_{hkl}) calculated using the Scherrer equation:[32]

$$L_{hkl} = \frac{K\lambda}{B\cos(\theta)} \tag{12}$$

where K and θ are the Scherrer factor (0.9) and peak position, respectively. The results are shown in Table III, which show that the crystallite sizes decreases with increasing 2.5 and 5 wt% nHA, indicating that nHA act as nucleus site. PBSET10-nHA1 doesn't follow the same trend and incorporating 1wt% nHA leads to increase in crystallite size possibly because of crystal perfection.[33]

The following equation was used to calculate the degree of crystallinity (χ_c) of all samples:

$$\chi_c = \left(\frac{\Delta H_m}{(\Delta H^0_{mS} \times \phi_1 + \Delta H^0_{mT} \times \phi_2) \times (1 - \phi_3)} \right) \times 100 \tag{13}$$

where ΔH_m is the heat of crystallization for PBSET10 in neat polymer and nanocomposites, and ΔH^0_{mS}, ΔH^0_{mT} are the heat of fusion for 100% crystalline PBS and PET which is 210 and 145 J/g, respectively.[12,34] ϕ_1, ϕ_2, and ϕ_3 are the weight

Table III. Quantitative Results of DSC and XRD Analysis

Sample	T_g (°C)	T_c (°C)	ΔH_c (J/g)	T_{cc} (°C)	ΔH_{cc} (J/g)	T_m (°C)	ΔT_m (°C)	χ_c (%)	n	Z_t	L_{110} (nm)
PBSET10-nHA0	-28.8	27.4	11.4	12.7	26.6	96.6	28.0	29.1	2.20	0.025	4.16
PBSET10-nHA1	-34.4	18.3	10.7	12.6	19.2	96.0	25.8	22.2	2.35	0.033	4.31
PBSET10-nHA2.5	-33.8	22.7	8.2	16.9	24.4	93.2	27.5	21.8	2.29	0.032	3.63
PBSET10-nHA5	-34.5	27.8	8.0	15.5	25.2	97.0	28.9	25.4	2.21	0.036	3.80

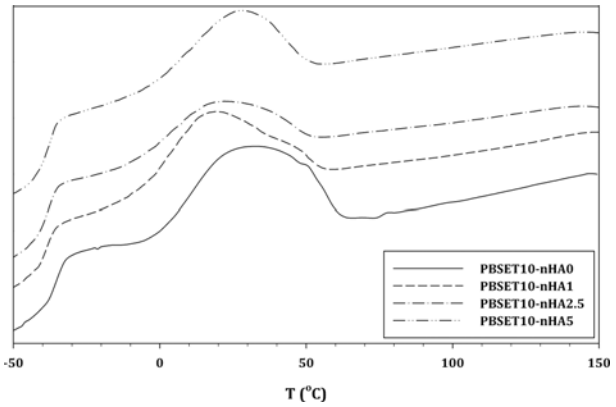

Figure 7. Cooling DSC thermograms of all samples.

percent of BS, ET, and nHA, respectively. The result is shown in Table III and indicates that the degree of crystallinity decrease with increasing nHA then increase which is the same as previous result and confirm the competition between increasing nucleation and decreasing chain mobility.

Cooling DSC curves (Figure 7) and its corrsponding data shows that ΔH_{cc} of nanocomposites is much higher than ΔH_c which indicates that the major part of crystallization happens in reheating. T_{cc} of the nanocomposites are 3-4 °C higher than those of PBSET10. This is due to the bonds between polymer chains and n-HA which limits the rearrangement of PBSET10 molecules, resulting in the increase of the crystallinity temperature. Moreover, the role of nHA as crystal nucleus leads to increase in maximum crystallization temperature.

Non-isothermal crystallization behavior of nanocomposites could be investigated using the modified Avrami equation:[35-37]

$$X_t = 1 - \exp(Z_t t^n) \quad \& \quad t = \frac{T_0 - T}{C} \tag{14}$$

where X_t, Z_t, n, and C are relative crystallinity at time t, growth rate constant, Avrami exponent and cooling rate, respectively. The following equation was used calculate relative crystallinity:

$$X_t = \frac{\int_{t_0}^{t} (dH_c/dt)dt}{\int_{t_0}^{t_\infty} (dH_c/dt)dt} \tag{15}$$

where t_0 and t_∞ are the initial and end times of crystallization, respectively. Figure 8 shows relative crystallinity versus time for all nanocomposites. The shape of all curves is the same and confirms that higher nanoparticle content leads to the higher crystallization rate. To calculate Ozawa constants, ln[-ln(1-X_t)] were plotted against ln$t$, which is shown in Figure 9. The curves are linear in the range of 10-80% of relative crystallinity. Slopes and intercepts of the lines are Avrami exponent (n) and growth rate constant (Z_t), respectively, which are listed in

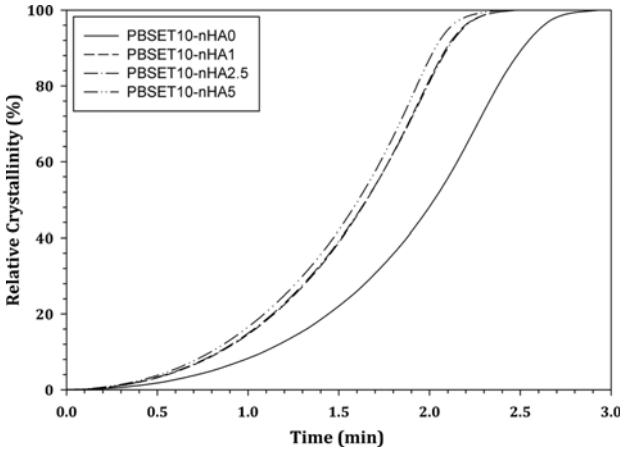

Figure 8. Relative crystallinity of all nanocomposites.

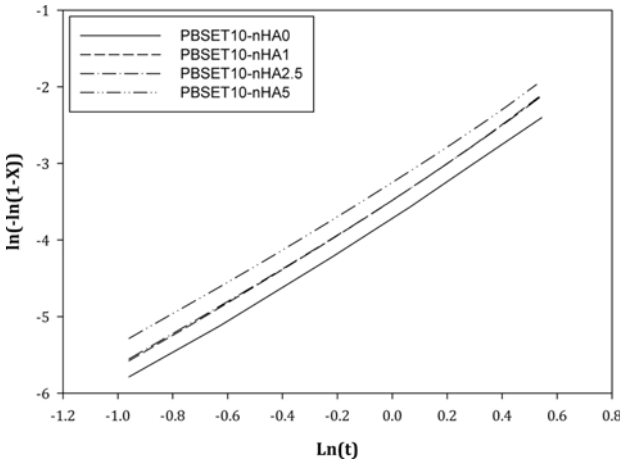

Figure 9. Double logarithm curves of modified Avrami equation.

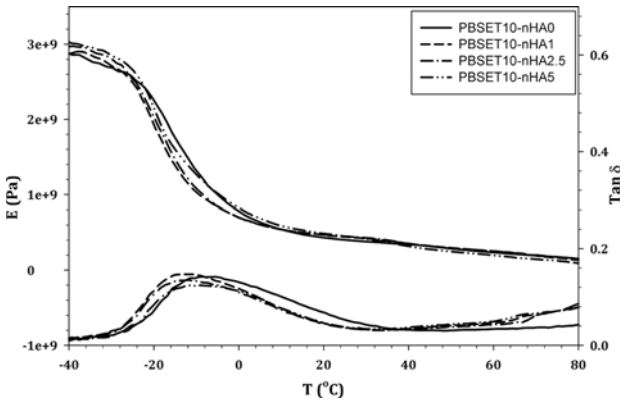

Figure 10. DMTA curves of all synthesized samples.

Table III. Avrami exponent are in the range of 2.20-2.35, which indicates that nanocomposites crystal are in spherical form.[38] Moreover, Z_t values increase with the addition of nHA, confirmed the increasing of crystallization rate. For nanocomposites, nHA acts as crystal nucleus and molecular chains

Table IV. Quantitative Results of DMTA and Tensile Analysis

Sample	T_g	E (MPa)			σ (MPa)	Elongation @ Break
		-40 °C	25 °C	37 °C		
PBSET10-nHA0	-7.7	2,887	403.9	353.3	27.7	587.3
PBSET10-nHA1	-12.5	2,871	441.7	373.9	27.0	523.6
PBSET10-nHA2.5	-12.7	2,997	447.7	381.7	29.3	524.4
PBSET10-nHA5	-10.8	3,045	453.9	343.7	29.8	503.9

arrange rapidly at T_c which leads to increase in crystallization rate.

DMTA results of nanocomposites and their quantitative data are shown in Figure 10 and Table IV, respectively. The glass transition temperatures of nanocomposites, which is the peak of tanδ, are lower than that of PBSET10 due to the repulsive interaction at the filler-polymer interface and confirm DSC results. Moreover, the broadening of relaxation peak, which is related to increase in crystallinity, indicate that crystallinity decrease with increasing 1% nHA and then increase with 2.5 and 5% nHA and confirmed previous results. Furthermore, it was reported that the intensity of tanδ peak decreases with the restriction of polymer chains mobility due to the presence of nanoparticle.[39] Storage modulus curves show a slight increase with the nanoparticles weight fraction below the glass transition temperature, then decreases and increases in the range of -25 to 10 °C and it is almost the same above 10 °C for all nanocomposites. Increase in crystallization degree or mixing polymer with hard particles leads to increase in storage modulus.[40,41] As mentioned before, nanocomposites show lower crystallinity than PBSET10. Therefore, increasing of the nanoparticles weight fraction and decreasing crystallinity compete to change storage modulus. DMTA and tensile results show that storage modulus and tensile strength increase with nHA content, and elongation at break slightly decreases, but incorporation of 1 wt% nHA leads to decrease in storage modulus at -40 and 25 °C which shows that the reduction of crystallinity can overcome the increase of nanoparticle content.

Figure 11 and Table V show *in vitro* degradation of nanocomposites in NaOH solution. Chemical structure and surrounding environment affect hydrolytic degradation of polyesters. Nanocomposites weight loss depends on water diffusion, chain scission rate and removal of the resulted oligomers.[42] Based on the degradation results, the following equation was used to investigate the hydrolysis kinetics:

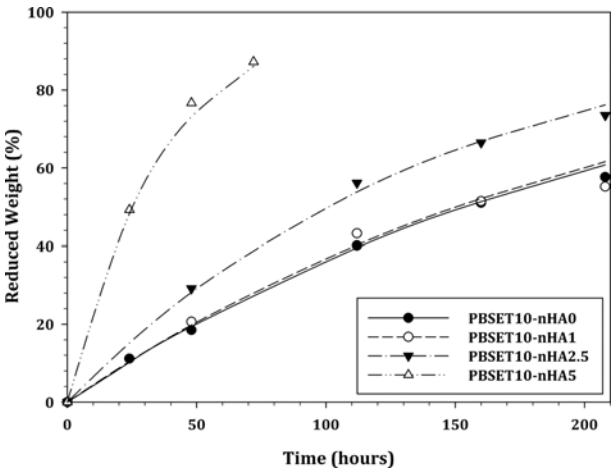

Figure 11. Hydrolytic degradation of all synthesized samples.

$$W = 100 \times (1 - \exp(-kt)) \tag{16}$$

where W, k and t are the weight loss percentage, degradation rate constant and time, respectively. Moreover, $t_{1/2}$ which is the time that polymer degrades to half of its initial weight, is given in Table V.

Number of ester groups, hydrophilicity, crystallinity and the surface area are the main parameters that affect the degradation rate.[42,43] As it was expected, incorporating hydrophilic nHA into PBSET10 dramatically increases the hydrolytic degradability. Moreover, reduction in crystallinity and crystallite size, according to DSC and XRD data, is observed in higher degradability. However, the close result of PBSET10-nHA0 and PBSET10-nHA1 means incorporating 1 wt% nHA slightly increases the hydrophilicity which leads to slightly increase in hydrolytic degradation. Consequently, we may have a nanocomposite with a tuneable degradation time.

Table V. *In Vitro* Hydrolysis Results of All Samples

	PBSET10-nHA0	PBSET10-nHA1	PBSET10-nHA2.5	PBSET10-nHA5
k (1/h)	0.0045	0.0046	0.0069	0.0274
R^2	0.9963	0.9775	0.9963	0.9969
$t_{1/2}$ (h)	154.0	150.7	100.5	25.3

Conclusions

PBSET10-nHA nanocomposites with 1, 2.5, and 5 wt% of nano hydroxyapatite were synthesized by *in situ* polycondensation of BHET, and BHBS, produced by esterification of 1,4-butanediol, ethylene glycol, succinic acid and terephthalic acid, and nHA. Generally, the properties of nanocomposites were enhanced when compared to the neat PBSET10. ^{1}H NMR results show that introducing nHA doesn't have any effect on molecular sequences length but there is a chemical bond between nHA and polymer. TEM images show the good dispersion of nHA in nanocomposites. DSC, XRD, and Ozawa equations were used to study crystal morphology, which indicated that the introduction of nHA leads to decrease in the crystallinity degree, melting point and the glass transition temperature, due to the grafting nHA to polymer chain, decrement of chain mobility and increase in nucleus sites. Higher elastic modulus, lower elongation at break and higher tensile strength of nanocomposites were compared to their parent polymer obtained by mechanical analysis investigations. Greater hydrophilicity, more crystallization rate and smaller crystallite size of nanocomposites are the main reasons of higher hydrolytic degradation rate.

References

(1) Y. J. Phua, N. S. Lau, K. Sudesh, W. S. Chow, and Z. M. Ishak, *J. Compos. Mater.*, **49**, 891 (2015).
(2) X. Li and Z. Qiu, *Macromol. Res.*, **23**, 678 (2015).
(3) Y. Sung, T. H. Kim, and B. Lee, *Macromol. Res.*, **24**, 143 (2016).
(4) Y. Huang, X. Niu, L. Wang, X. Li, G. Zhou, Q. Feng, J. Fan, and Y. Fan, *J. Compos. Mater.*, **48**, 1971 (2014).
(5) A. N. Koo, J. Y. Ohe, D. W. Lee, J. Chun, H. J. Lee, Y. D. Kwon, and S. C. Lee, *Macromol. Res.*, **23**, 1168 (2015).
(6) S. Zhan, J. Wang, Q. Qi, M. Li, W. Wang, S. Ding, and S. Chen, *J. Polym. Res.*, **22**, 161 (2015).
(7) B. Laycock, P. Halley, S. Pratt, A. Werker, and P. Lant, *Prog. Polym. Sci.*, **38**, 536 (2013).
(8) Y. J. Kim, G. D. Kang, K. C. Yoon, Y. Hwang, and O. Park, *Macromol. Res.*, **23**, 887 (2015).
(9) D. N. Bikiaris and D. S. Achilias, *Polymer*, **49**, 3677 (2008).
(10) G. H. Eshaq and A. E. ElMetwally, *J. Mol. Liquids*, **214**, 1 (2016).
(11) S. L. Li, F. Wu, Y. Yang, Y. Z. Wang, and J. B. Zeng, *Polym. Adv. Technol.*, **26**, 1003 (2015).
(12) H. Shirali, M. Rafizadeh, and F. A. Taromi, *Macromol. Res.*, **23**, 755 (2015).
(13) C. Harms, K. Helms, T. Taschner, I. Stratos, A. Ignatius, T. Gerber, S. Lenz, S. Rammelt, B. Vollmar, and T. Mittlmeier, *Int. J. Nanomed.*, **7**, 2883 (2012).
(14) S. Dadbin and F. Naimian, *Polym. Int.*, **63**, 1063 (2014).
(15) Z. C. Xing, S. J. Han, Y. S. Shin, and I. K. Kang, *J. Nanomater.*, **2011** (2011).
(16) H. R. Kricheldorf, *Chem. Rev.*, **109**, 5579 (2009).
(17) R. A. Gross, M. Ganesh, and W. Lu, *Trends Biotechnol.*, **28**, 435 (2010).
(18) R. R. Fan, L. X. Zhou, W. Song, D. X. Li, D. M. Zhang, Y. Zheng, G. Guo, and R. Ye, *Int. J. Biol. Macromol.*, **59**, 227 (2013).
(19) V. Tserki, P. Matzinos, E. Pavlidou, and C. Panayiotou, *Polym. Degrad. Stab.*, **91**, 377 (2006).
(20) M. Soccio, N. Lotti, M. Gigli, L. Finelli, M. Gazzano, and A. Munari, *Polym. Int.*, **61**, 1163 (2012).
(21) R. S. Loup, T. Jeanmaire, J. J. Robin, and B. Boutevin, *Polymer*, **44**, 3437 (2003).
(22) C. H. Chen, H. Y. Lu, M. Chen, J. S. Peng, C. J. Tsai, and C. S. Yang, *J. Appl. Polym. Sci.*, **111**, 1433 (2009).
(23) R. N. Panda, M. F. Hsieh, R. J. Chung, and T. S. Chin, *J. Phys. Chem. Solids*, **64**, 193 (2003).
(24) S. Gandhi, S. Sethuraman, and U. M. Krishnan, *Macromol. Res*., **21**, 833 (2013).
(25) A. Jayaraman, *J. Polym. Sci., Part B: Polym. Phys.*, **51**, 524 (2013).
(26) H. J. Lee, S. E. Kim, H. W. Choi, C. W. Kim, K. J. Kim, and S. C. Lee, *Eur. Polym. J.*, **43**, 1602 (2007).
(27) B. K. Money, K. Hariharan, and J. Swenson, *J. Phys. Chem. B*, **116**, 7762 (2012).
(28) A. Bansal, H. Yang, C. Li, K. Cho, B. C. Benicewicz, S. K. Kumar, and L. S. Schadler, *Nature*, **4**, 693 (2005).
(29) X. Zhang, Y. Li, G. Lv, Y. Zuo, and Y. Mu, *Polym. Degrad. Stab.*, **91**, 1202 (2006).
(30) M. S. Nikolic and J. Djonlagic, *Polym. Degrad. Stab.*, **74**, 263 (2001).
(31) Y. X. Pang and X. Bao, *J. Eur. Ceram. Soc.*, **23**, 1697 (2003).
(32) K. M. Choi, S. W. Lim, M. C. Choi, D. H. Han, and C. S. Ha, *Macromol. Res.*, **22**, 1312 (2014).
(33) M. R. Khan, H. Mahfuz, T. Leventouri, V. K. Rangari, and A. Kyriacou, *Polym. Eng. Sci.*, **51**, 654 (2011).
(34) S. D. Hoyo-Gallego, L. Pérez-Álvarez, F. Gómez-Galván, E. Lizundia, I. Kuritka, V. Sedlarik, J. M. Laza, and J. L. Vila-Vilela, *Carbohydr. Polym.*, **143**, 35 (2016).
(35) A. Bahader, H. Gui, Y. Li, P. Xu, and Y. Ding, *Macromol. Res.*, **23**, 273 (2015).
(36) S. N. Sheikholeslami, M. Rafizadeh, F. A. Taromi, and H. Bouhendi, *J. Thermoplast. Compos*., **27**, 1530 (2014).
(37) H. A. M. Saeed, Y. A. Eltahir, Y. Xia, and W. Yimin, *Polym. Bull.*, **71**, 595 (2014).
(38) J. D. Menczel and R. B. Prime, in *Thermal Analysis of Polymers: Fundamentals and Applications*, Wiley, 2009, Chap. 2.
(39) H. Shirali, M. Rafizadeh, and F. A. Taromi, *J. Compos. Mater.*, **48**, 301 (2014).
(40) X. Deng, J. Hao, and C. Wang, *Biomaterials*, **22**, 2867 (2001).
(41) Y. Srithep, P. Nealey, and L. S. Turng, *Polym. Eng. Sci*., **53**, 580 (2013).
(42) S. N. Sheikholeslami, M. Rafizadeh, F. A. Taromi, H. Shirali, and E. Jabbari, *Polymer*, **98**, 70 (2016).
(43) D. Barati, S. Moeinzadeh, O. Karaman, and E. Jabbari, *Polymer*, **55**, 3894 (2014).